REPORT DOCUMENTATION PAGE

Form Approved OMB NO. 0704-0188

1. REPORT DATE (DD-MM-YYYY)	2. REPORT TYPE	3. DATES COVERED (From - To)
09-02-2016	Final Report	10-Aug-2011 - 9-Aug-2015

4. TITLE AND SUBTITLE
Final Report: Identification and Manipulation of Novel Topological Phases

5a. CONTRACT NUMBER
W911NF-11-1-0331

5b. GRANT NUMBER

5c. PROGRAM ELEMENT NUMBER
611102

6. AUTHORS
Nuh Gedik

5d. PROJECT NUMBER

5e. TASK NUMBER

5f. WORK UNIT NUMBER

7. PERFORMING ORGANIZATION NAMES AND ADDRESSES
Massachusetts Institute of Technology (MIT
77 Massachusetts Ave.
NE18-901
Cambridge, MA 02139 -4307

8. PERFORMING ORGANIZATION REPORT NUMBER

9. SPONSORING/MONITORING AGENCY NAME(S) AND ADDRESS (ES)
U.S. Army Research Office
P.O. Box 12211
Research Triangle Park, NC 27709-2211

10. SPONSOR/MONITOR'S ACRONYM(S)
ARO

11. SPONSOR/MONITOR'S REPORT NUMBER(S)
60056-PH.3

12. DISTRIBUTION AVAILIBILITY STATEMENT
Approved for Public Release; Distribution Unlimited

13. SUPPLEMENTARY NOTES
The views, opinions and/or findings contained in this report are those of the author(s) and should not contrued as an official Department of the Army position, policy or decision, unless so designated by other documentation.

14. ABSTRACT
The goal of this award was identifying and manipulating novel topological phases. It has three main thrusts: 1) Searching for new topological electronic phases and directly visualizing topological spin currents using time-resolved photoelectron spectroscopy; 2) Measuring topological order through photo-induced currents; and 3) Probing new emergent phases at topological/non-topological materials interfaces using ultrafast non-linear spectroscopies. In this report, we describe some of the achievements under this award.

15. SUBJECT TERMS

16. SECURITY CLASSIFICATION OF:			17. LIMITATION OF ABSTRACT	15. NUMBER OF PAGES	19a. NAME OF RESPONSIBLE PERSON
a. REPORT	b. ABSTRACT	c. THIS PAGE			Nuh Gedik
UU	UU	UU	UU		19b. TELEPHONE NUMBER 617-253-3420

Standard Form 298 (Rev 8/98)
Prescribed by ANSI Std. Z39.18

Report Title

Final Report: Identification and Manipulation of Novel Topological Phases

ABSTRACT

The goal of this award was identifying and manipulating novel topological phases. It has three main thrusts: 1) Searching for new topological electronic phases and directly visualizing topological spin currents using time- resolved photoelectron spectroscopy; 2) Measuring topological order through photo-induced currents; and 3) Probing new emergent phases at topological/non-topological materials interfaces using ultrafast non-linear spectroscopies. In this report, we describe some of the achievements under this award.

Enter List of papers submitted or published that acknowledge ARO support from the start of the project to the date of this printing. List the papers, including journal references, in the following categories:

(a) Papers published in peer-reviewed journals (N/A for none)

Received		Paper
07/18/2012	1.00	D. Hsieh, F. Mahmood, D. H. Torchinsky, G. Cao, N. Gedik. Observation of a metal-to-insulator transition with both Mott-Hubbard and Slater characteristics in Sr2IrO4 from time-resolved photocarrier dynamics, Physical Review B, (07 2012): 35128. doi:
TOTAL:	**1**	

Number of Papers published in peer-reviewed journals:

(b) Papers published in non-peer-reviewed journals (N/A for none)

Received		Paper
02/09/2016	2.00	Fahad Mahmood, , Zhanybek Alpichshev, , Gang Cao, , Nuh Gedik. Confinement-Deconfinement Transition as an Indication of Spin-Liquid-Type Behavior in Na2IrO3, PHYSICAL REVIEW Letters, (01 2015): 17203. doi:
TOTAL:	**1**	

Number of Papers published in non peer-reviewed journals:

(c) Presentations

Number of Presentations: 0.00

Non Peer-Reviewed Conference Proceeding publications (other than abstracts):

Received Paper

TOTAL:

Number of Non Peer-Reviewed Conference Proceeding publications (other than abstracts):

Peer-Reviewed Conference Proceeding publications (other than abstracts):

Received Paper

TOTAL:

Number of Peer-Reviewed Conference Proceeding publications (other than abstracts):

(d) Manuscripts

Received Paper

TOTAL:

Number of Manuscripts:

Books

Received Book

TOTAL:

Received Book Chapter

TOTAL:

Patents Submitted

Patents Awarded

Awards

Moore Experimental Investigator in Quantum Materials (2015-2020)
DARPA Young Faculty Award (2013)
Biedenharn Career Development Professorship (2012-2015)
Plenary Speaker, 3rd. International Conference in Superconductivity and Magnetism (ICSM2012) Alfred P. Sloan Fellowship (2012-2014)

Graduate Students

NAME	PERCENT_SUPPORTED	Discipline
James McIver	0.17	
Daniel Pilon	0.13	
Fahad Mahmood	0.13	
Edbert Jarvis Sie	0.13	
FTE Equivalent:	**0.56**	
Total Number:	**4**	

Names of Post Doctorates

NAME	PERCENT_SUPPORTED
Zhanybek Alpichshev	0.00
FTE Equivalent:	**0.00**
Total Number:	**1**

Names of Faculty Supported

NAME	PERCENT_SUPPORTED	National Academy Member
Nuh Gedik	0.13	
FTE Equivalent:	**0.13**	
Total Number:	**1**	

Names of Under Graduate students supported

NAME	PERCENT_SUPPORTED
FTE Equivalent:	
Total Number:	

Student Metrics

This section only applies to graduating undergraduates supported by this agreement in this reporting period

The number of undergraduates funded by this agreement who graduated during this period: 0.00

The number of undergraduates funded by this agreement who graduated during this period with a degree in science, mathematics, engineering, or technology fields:..... 0.00

The number of undergraduates funded by your agreement who graduated during this period and will continue to pursue a graduate or Ph.D. degree in science, mathematics, engineering, or technology fields:..... 0.00

Number of graduating undergraduates who achieved a 3.5 GPA to 4.0 (4.0 max scale):..... 0.00

Number of graduating undergraduates funded by a DoD funded Center of Excellence grant for Education, Research and Engineering:..... 0.00

The number of undergraduates funded by your agreement who graduated during this period and intend to work for the Department of Defense 0.00

The number of undergraduates funded by your agreement who graduated during this period and will receive scholarships or fellowships for further studies in science, mathematics, engineering or technology fields:..... 0.00

Names of Personnel receiving masters degrees

NAME
Total Number:

Names of personnel receiving PHDs

NAME
James McIver
Total Number: 1

Names of other research staff

NAME	PERCENT_SUPPORTED
FTE Equivalent:	
Total Number:	

Sub Contractors (DD882)

Inventions (DD882)

Scientific Progress

We have been working on identifying topological phases in iridate compounds in which an intricate interplay between spin-orbit interactions, crystal field splitting and coulomb repulsion of 5d electrons. We had two significant achievements under this grant. First, we used time-resolved optical spectroscopy, which is highly sensitive to the existence of energy gaps, to study the temperature evolution of the electronic structure of Sr2IrO4 . Taking advantage of qualitatively distinct relaxation dynamics of photoexcited carriers exhibited by gapped and gapless systems, we find a clear change in the ultrafast dynamics across TN indicating a gap opening concomitant with antiferromagnetic order. Analysis of the long-time relaxation dynamics further reveals behavior that is consistent with in-gap spectral weight being continuously transferred to high energies through TN , supporting a phase transition from low-temperature insulator to high-temperature paramagnetic metal with both Mott- Hubbard and Slater-type characteristics.

Secondly, we observed the confinement of single particle excitations and a confinement to deconfinement transition in a layered, quasi-2D, strongly frustrated antiferromagnetic Na2IrO3 iridate system. Recently several research groups conjectured that these materials might be an experimental realization of the Kitaev model of a spin liquid. Although it was experimentally shown that this system does undergo ordering at relatively low temperatures (T=15K) and hence is not a spin liquid, it was demonstrated it is still a highly frustrated spin system.

For the details of these achivements, please refer to the attached papers. We are also including a short summary of the unpublished results describing work done after our latest publication.

Technology Transfer

Observation of a metal-to-insulator transition with both Mott-Hubbard and Slater characteristics in Sr_2IrO_4 from time-resolved photocarrier dynamics

D. Hsieh,[1] F. Mahmood,[1] D. H. Torchinsky,[1] G. Cao,[2,3] and N. Gedik[1]
[1]*Department of Physics, Massachusetts Institute of Technology, Cambridge, Massachusetts 02139, USA*
[2]*Center for Advanced Materials, University of Kentucky, Lexington, Kentucky 40506, USA*
[3]*Department of Physics and Astronomy, University of Kentucky, Lexington, Kentucky 40506, USA*
(Received 20 March 2012; published 18 July 2012)

We perform a time-resolved optical study of Sr_2IrO_4 to understand the influence of magnetic ordering on the low energy electronic structure of a strongly spin-orbit coupled $J_{\text{eff}} = 1/2$ Mott insulator. By studying the recovery dynamics of photoexcited carriers, we find that upon cooling through the Néel temperature T_N the system evolves continuously from a metal-like phase with fast (∼50 fs) and excitation density independent relaxation dynamics to a gapped phase characterized by slower (∼500 fs) excitation density-dependent bimolecular recombination dynamics, which is a hallmark of a Slater-type metal-to-insulator transition. However our data indicate that the high energy reflectivity associated with optical transitions into the unoccupied $J_{\text{eff}} = 1/2$ band undergoes the sharpest upturn at T_N, which is consistent with a Mott-Hubbard type metal-to-insulator transition involving spectral weight transfer into an upper Hubbard band. These findings show Sr_2IrO_4 to be a unique system in which Slater- and Mott-Hubbard-type behaviors coexist and naturally explain the absence of anomalies at T_N in transport and thermodynamic measurements.

DOI: 10.1103/PhysRevB.86.035128 PACS number(s): 71.27.+a, 71.70.Ej, 78.47.−p

I. INTRODUCTION

Iridium oxides are unique 5*d* electronic systems in which spin-orbit coupling, electronic bandwidth (W), and on-site Coulomb interactions (U) occur on comparable energy scales. Their interplay can stabilize a novel $J_{\text{eff}} = 1/2$ Mott insulating state in which a correlation gap is opened by only moderate Coulomb interactions owing to a spin-orbit coupling induced band narrowing.[1] Depending on the underlying lattice, this insulating state is predicted to realize a variety of exotic quantum phases including antiferromagnetic $J_{\text{eff}} = 1/2$ Mott insulators on the perovskite lattice,[1–3] correlated topological insulators and semimetals on the pyrochlore lattice,[4–6] and topological spin liquids on the hyper-kagome[7] and honeycomb lattices.[8] Even more tantalizing possibilities are predicted to occur upon chemically doping these systems, ranging from high-T_c superconductivity[9,10] to spin-triplet superconductivity.[8]

Intensive research has been conducted on the layered perovskite iridate Sr_2IrO_4 owing to its structural and electronic similarities to undoped high-T_c cuprates such as La_2CuO_4.[1,9] The ground-state electronic structure of Sr_2IrO_4 consists of a completely filled band with total angular momentum $J_{\text{eff}} = 3/2$ and a narrow half-filled $J_{\text{eff}} = 1/2$ band near the Fermi level E_F.[1,11,12] The latter is split into an upper Hubbard band (UHB) and lower Hubbard band (LHB) due to on-site Coulomb interactions and exhibits antiferromagnetic ordering of the effective $J_{\text{eff}} = 1/2$ moments below a Néel temperature $T_N = 240$ K[3] analogous to La_2CuO_4. Although this insulating ground state has been established by angle-resolved photoemission spectroscopy[1] and resonant x-ray scattering[11] measurements, whether Sr_2IrO_4 is a Mott-type ($U \gg W$) insulating phase typical of 3*d* transition metal oxides or a Slater-type ($U \approx W$) insulating phase is experimentally unknown and remains a topic of active theoretical debate.[10,13,14] Whereas a Mott-Hubbard-type metal-to-insulator transition (MIT) is discontinuous and occurs at temperatures greater or equal to T_N, a Slater-type MIT is continuous and occurs exactly at T_N.[15] Therefore the relevant experimental question is whether heating above T_N brings Sr_2IrO_4 into a paramagnetic insulating phase or into a paramagnetic metallic phase and what the order of the MIT is.

Owing to an absence of clear anomalies at T_N in transport,[3,16–18] thermodynamic,[17] and optical conductivity data,[19] there have been conflicting interpretations about how the insulating gap behaves across T_N. In this article we use time-resolved optical spectroscopy, which is highly sensitive to the existence of energy gaps,[20,21] to study the temperature evolution of the electronic structure of Sr_2IrO_4. Taking advantage of qualitatively distinct relaxation dynamics of photoexcited carriers exhibited by gapped and gapless systems, we find a clear change in the ultrafast dynamics across T_N indicating a gap opening concomitant with antiferromagnetic order. Analysis of the long-time relaxation dynamics further reveals behavior that is consistent with in-gap spectral weight being continuously transferred to high energies through T_N, supporting a phase transition from low-temperature insulator to high-temperature paramagnetic metal with both Mott-Hubbard and Slater-type characteristics.

II. EXPERIMENTAL DETAILS

In our experiment we used a Ti:sapphire oscillator producing laser pulses with center wavelength 795 nm ($h\nu = 1.56$ eV) and near 80 fs duration. The fluence of the pump pulse, which excites electrons across the insulating gap from the occupied $J_{\text{eff}} = 3/2$ and $J_{\text{eff}} = 1/2$ bands to the unoccupied $J_{\text{eff}} = 1/2$ band [inset Fig. 1(a)], was varied with neutral density filters to tune the photoexcited carrier density while the probe fluence was maintained at 4 μJ/cm^2. Both beams were focused to a 70-μm full width at half maximum (FWHM) spot on the (001) cleaved face of the sample. The 80-MHz repetition rate was reduced to 1.6 MHz with a pulse picker to eliminate steady-state heating of the sample. Use of a

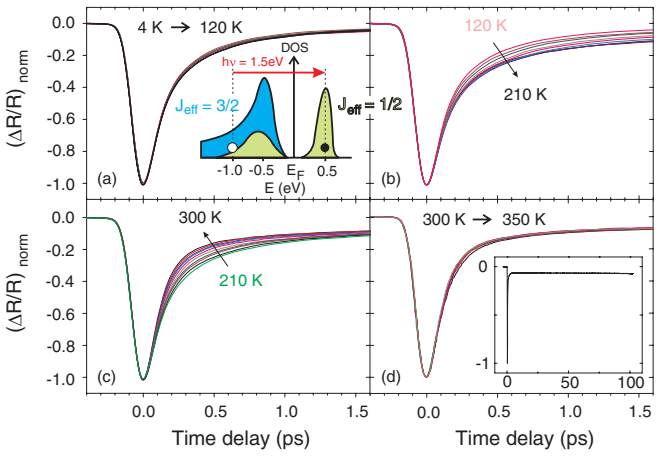

FIG. 1. (Color) Normalized time-resolved reflectivity traces $(\Delta R/R)_{\text{norm}}$ of Sr_2IrO_4 collected in the temperature ranges (a) 4–120 K, (b) 120–210 K, (c) 210–300 K, and (d) 300–350 K. Curves are collected in 10-K intervals with a pump fluence of 15.4 μJ/cm^2. Inset of panel (a) shows a schematic of the low-energy electronic density of states (DOS) based on calculations.[12] The red arrow denotes the optical transition being excited by the pump pulse. Inset of panel (d) shows the $T = 300$ K trace out to 100-ps time delay.

double-modulation scheme[20] provided sensitivity to the fractional change of reflectivity on the order $\Delta R/R \sim 10^{-7}$. Single crystals of Sr_2IrO_4 were grown using a self-flux technique and magnetization measurements show a magnetic ordering temperature at $T_N = 240$ K.[3,17]

III. RESULTS AND ANALYSIS

Figure 1 shows typical time-resolved reflectivity transients measured over a range of temperatures spanning 4–350 K, which have all been normalized to their negative peak values in order to emphasize the recovery dynamics. We note that the temperature here refers to that before the pump excitation, which will be lower than the instantaneous electronic temperatures reached in the ps time windows following photoexcitation. Following the pump excitation, the electronic temperature is elevated above the initial equilibrium temperature and all $\Delta R/R$ traces exhibit a rapid negative spike, which indicates a decrease in reflectivity. Within approximately 1 ps, the reflectivity recovers to a small negative offset that persists beyond 100 ps [Fig. 1(d) inset]. By performing a temperature dependence study we find that the initial ~1-ps recovery can actually be decomposed into two separate components as follows. Figure 1(a) shows that between 4 and 120 K there is no discernible change in the recovery dynamics. Upon heating from 120 to 210 K [Fig. 1(b)], we find no temperature dependence within the first ~100 fs but observe a clear slowing down of recovery dynamics after this time. Further heating of the sample from 210 to 300 K again causes no change in the first recovery component but causes the second component to become faster [Fig. 1(c)]. All temperature dependence then completely shuts off above 300 K [Fig. 1(d)]. To understand the physical processes underlying these trends, we perform detailed fits to the $\Delta R/R$ traces.

We fit the un-normalized time-resolved reflectivity transients $[\Delta R/R](t)$ at all temperatures to a convolution $[f \otimes g](t) \equiv \int_{-\infty}^{\infty} f(\xi)g(t-\xi)d\xi$ of a bi-exponential decay function $f(t)$ and a Gaussian instrument resolution function $g(t)$ where

$$f(t) = \begin{cases} 0; & \text{if} \quad t < 0 \\ \text{Ae}^{-t/\tau_1} + \text{Be}^{-t/\tau_2} + \text{C}; & \text{if} \quad t > 0, \end{cases}$$

and

$$g(t) = \frac{1}{\sigma\sqrt{2\pi}} e^{-\frac{t^2}{2\sigma^2}},$$

where σ is experimentally determined by measuring an autocorrelation of our laser pulses.

To demonstrate that the $[\Delta R/R](t)$ traces are described by a minimum of two exponential decays, we fit $[f \otimes g](t)$ to our data at positive time delays to both a single and double exponential decay. We show fits to the data in two extreme cases: (i) data taken at a temperature $T = 300$ K and pump fluence $F = 15.4$ μJ/cm^2, where the magnitude of the slower decay component is shown to be smallest [shown later in Fig. 4(c)], (ii) data taken at a temperature $T = 180$ K and pump fluence $F = 1.9$ μJ/cm^2, where the magnitude of the slower decay component is shown to be largest [shown later in Fig. 4(c)]. Figure 2 shows that in both extremes, the data can only be satisfactorily described by two exponential decays. A decomposition of the fits into its individual components (Fig. 2) shows that the slow component is required to account for the curvature in $\Delta R/R$ around 0.5 ps. The fitted parameters listed in red show that their standard error is small, less than the size of the symbols plotted in all the figures. We found that the fit results are not sensitive to changes of order ±40% in their initial estimated values.

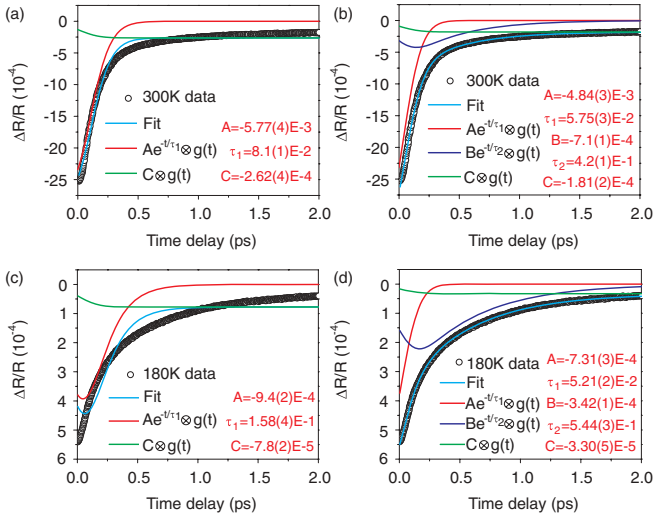

FIG. 2. (Color) Transient reflectivity traces taken at $T = 300$ K and $F = 15.4$ μJ/cm^2 and fitted to a (a) single and (b) double exponential decay. Transient reflectivity traces taken at $T = 180$ K and $F = 1.9$ μJ/cm^2 and fitted to a (c) single and (d) double exponential decay. Curves show the overall fit as well as the separate components of the fit. The fitted parameters and their associated fitting errors (in parentheses) are listed in red.

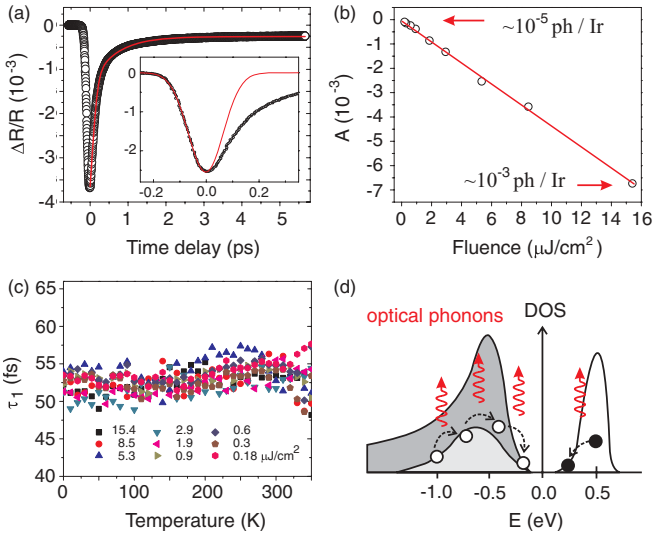

FIG. 3. (Color) (a) A typical un-normalized time-resolved reflectivity transient ($\Delta R/R$) of Sr_2IrO_4 overlaid with a bi-exponential fit described in the text (red curve). Inset shows the Gaussian instrument time resolution (red curve) superimposed on 300-K data where decay dynamics are dominated by the fast (τ_1) component [Fig. 4(b)]. This shows that the fast initial decay is not resolution limited. (b) The fitted amplitude (A) of the fast exponential decay component measured over a range of pump fluences corresponding to $\sim 10^{-5}$ to $\sim 10^{-3}$ pump photons per iridium atom. The red line is a linear fit. (c) Temperature dependence of the fitted decay time (τ_1) of the fast exponential decay component measured over a range of pump fluences. (d) Schematic showing that the initial fast decay process is governed by energy relaxation of photoexcited electrons and holes towards the band edges via optical phonon emission. The errors in the fit parameters are smaller than the size of the symbols.

A. Fast decay component

We begin by trying to understand the physical origin of the first decay component, which is resolved by our ultrashort laser pulses [Fig. 3(a)]. To investigate whether this fast decay arises from thermalization of photoexcited carriers via carrier-carrier scattering, whose rate should depend on the number of photoexcited carriers,[22] we measured τ_1 over a range of pump fluences spanning a photoexcitation density d between $\sim 10^{-5}$ to $\sim 10^{-3}$ photons per iridium site. We estimate d using the expression $d = \frac{N}{n\sigma\xi}$, where N is the number of photons per pump pulse, n is the number of iridium sites per unit volume, σ is the area of the sample illuminated by the pump pulse, and ξ is the optical penetration depth of photons with wavelength $\lambda = 795$ nm. The penetration depth ξ is derived through the Beer-Lambert law $\xi = \frac{\lambda}{4\pi k}$.[23] The extinction coefficient k, equal to the imaginary part of the index of refraction, can be calculated using Eq. (8) in Ref. 24 from the amplitude (R) and phase (ϕ) of the reflection coefficient of Sr_2IrO_4. We use available published values of R and ϕ from lightly Rh-doped Sr_2IrO_4 thin films,[25] whose optical conductivity spectrum is nearly identical to bulk single crystalline Sr_2IrO_4.

A linear behavior of the component amplitude (A) over this fluence range [Fig. 3(b)] shows that the number of photoexcited carriers is indeed proportional to the pump fluence. Figure 3(c) shows that $\tau_1 \approx 50$ fs exhibits no discernible fluence nor temperature dependence between 4 and 350 K. This implies that the initial decay is not caused by photocarrier thermalization but more likely by photocarrier cooling, and that this cooling is not mediated by thermally occupied phonons. The participation of magnons is also negligible because τ_1 is insensitive to T_N. Given that the fast time scale of τ_1 is consistent with typical optical phonon-mediated cooling processes and that the Debye temperature of Sr_2IrO_4[16] far exceeds our measurement temperatures, we conclude that the initial fast recovery of $\Delta R/R$ is due to the cooling of photoexcited carriers via generation of hot optical phonons [Fig. 3(d)].

B. Slow decay component

The initial fast recovery of $\Delta R/R$ is followed by a second slower decay component, whose amplitude (B) exhibits an upturn upon cooling the starting equilibrium temperature of the system through T_N and then ceases to grow further below a temperature $T_G = 175$ K [Fig. 4(a)]. The amplitude of the fast component (A) shows comparatively little temperature dependence [Fig. 4(a)], therefore the temperature dependence of their relative amplitude (B/A) is dominated by the features observed in B [Figs. 4(b) and 4(c)]. This indicates that at temperatures far above T_N the electronic energy relaxation occurs predominantly through the lone process of optical phonon generation described in Fig. 3 and that a separate relaxation mechanism grows near T_N before saturating below T_G. The decay time τ_2 shows a similar upturn upon cooling through T_N from around 0.36 ps at 350 K to 0.55 ps at T_G and then exhibits a marked change in temperature dependence below T_G [Fig. 4(d)]. A sharp rise in relaxation time at T_N typically signifies the development of an energy gap,[20,21] where a depletion of states around E_F greatly reduces the efficiency of photocarrier relaxation from above to below E_F.

The hallmark of a fully formed energy gap is that photoexcited occupied states above E_F and empty states below E_F can only combine in a pairwise fashion. Therefore, unlike in a metal, the recombination rate should be proportional to the density of photoexcited electron-hole pairs.[26] We find that a clear fluence dependence of τ_2 develops only below T_G [Fig. 4(d)] and that the low-temperature relaxation rate τ_2^{-1} indeed increases linearly with fluence below 5 μJ/cm^2 [Fig. 4(e)]. This shows that below T_G, τ_2 represents the time scale for recombination of photoexcited electron-hole pairs across the insulating gap, which in the Mott-Hubbard limit corresponds to the recombination of empty and doubly occupied sites [inset Fig. 4(e)]. This ultrafast sub-ps recombination time in Sr_2IrO_4 is comparable to that observed in the two-dimensional (2D) antiferromagnetic cuprate Mott insulators,[27] which has been attributed to additional recombination channels involving hot magnon generation. Altogether these observations allow us to conclude that at temperatures far above T_N the system behaves like a metal. Near T_N the density of states around E_F is continually depleted upon cooling, which is consistent with optical conductivity measurements,[19] and the insulating gap is fully developed below T_G.

To rule out the possibility that the observed temperature-dependent features are artifacts of cross correlation between our five fitting parameters, we note that based on Figs. 3(c) and 4(a) the parameters A and τ_1 exhibit no pronounced features at the temperatures of interest T_N and T_G. Moreover, we show

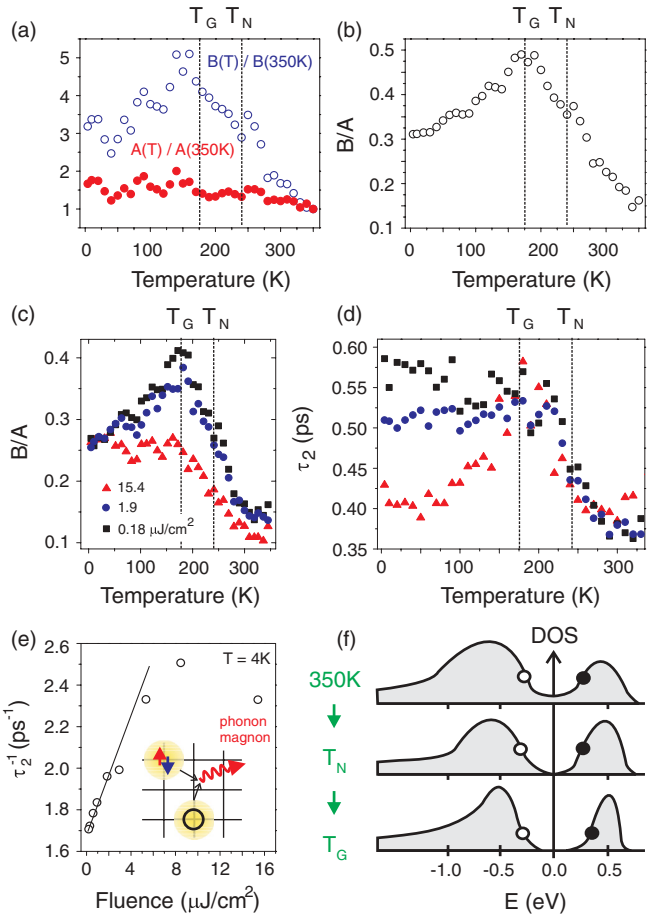

FIG. 4. (Color) (a) Temperature dependence of the fit parameters A and B, normalized to their values at $T = 350$ K, taken in the low pump fluence regime. (b) Temperature dependence of B/A derived from data shown in (a). (c) Temperature dependence of the amplitude ratio and (d) the decay time of the slower component (τ_2) measured using three different fluences 15.4 μJ/cm^2, 1.9 μJ/cm^2, and 0.18 μJ/cm^2. (e) Fluence dependence of the slower decay rate measured at 4 K. Straight line is a guide to the eye showing a linear dependence at low fluences. The errors in the fit parameters are less than the size of the symbols. A schematic of the bimolecular relaxation process involving the annihilation of photoexcited empty and doubly occupied sites via emission of optical phonons or magnons is shown in the inset, which emphasizes the Mott-Hubbard character of the system. (f) Schematic showing the temperature evolution of the low-energy electronic density of states (DOS) in Sr_2IrO_4 based on our data. Filled and empty circles denote the photoexcited electron and hole respectively.

in the following section that the feature at T_N observed in the temperature dependence of C is completely independent of the fitted parameters associated with the two exponential decays. Therefore the only parameters that show features at T_N and T_G and may be interdependent are B and τ_2. However, the fitting errors associated with B and τ_2 are very small (Fig. 2), which is further support that their temperature dependence is real and robust.

The occurrence of the metal-to-insulator transition at T_N in Sr_2IrO_4 (Fig. 4) distinguishes it from archetypal Mott insulators such as MnO where the insulating gap persists even in the absence of long-range magnetic order.[28] The continuous nature of the MIT and its development over a broad ($0.7 \lesssim T/T_N \lesssim 1.4$) temperature window further precludes a Mott-Hubbard description, which predicts sharp first-order MITs like in V_2O_3.[28] Although our measurements do not rule out gaps beginning to form in microscopically segregated regions above a bulk MIT temperature (T_{MIT}), such as the case in doped V_2O_3,[29] the fact that such gap opening takes place exactly across T_N in Sr_2IrO_4 defies a strict Mott-Hubbard description. We rule out the possibility of a disorder broadened T_{MIT} in our samples based on their sharp magnetic susceptibility curves.[3,17] Although these results point towards a second-order Slater-type MIT, Sr_2IrO_4 does not conform to a weakly correlated ($U \ll W$) spin-density wave description, which are driven purely by Fermi surface nesting and are typically only partially gapped below T_N. Unlike a conventional spin-density wave system, magnetic ordering in Sr_2IrO_4 does not change the size of the unit cell[11] and local moment fluctuations exist well above T_N according to both magnetic susceptibility[3,17] and magnetic diffuse x-ray scattering measurements.[30] While these magnetic signatures provide evidence for correlation physics at play, a direct electronic distinction between a correlation driven MIT and a Fermi surface nesting driven MIT is whether or not, respectively, spectral weight is transferred from low (near E_F) energies to high (of order U) energies upon traversing the MIT.[31]

C. Offset component

To determine whether the in-gap spectral weight lost at T_N is being transferred to upper and lower Hubbard bands, we investigate the temperature dependence of the optical reflectivity at the energy scale of optical transitions from the occupied $J_{\text{eff}} = 1/2$ and $J_{\text{eff}} = 3/2$ bands to the unoccupied $J_{\text{eff}} = 1/2$ band [inset Fig. 1(a)] by studying the small negative offset term C in the un-normalized $\Delta R/R$ traces. The two exponential relaxation processes have been identified as intraband cooling and recombination processes that both lead to a transfer of energy from the electronic to lattice subsystems, which brings them into thermal equilibrium within the first few ps [Fig. 5(a)]. Subsequent cooling of this heated sample spot back to the initial temperature takes place through the diffusion

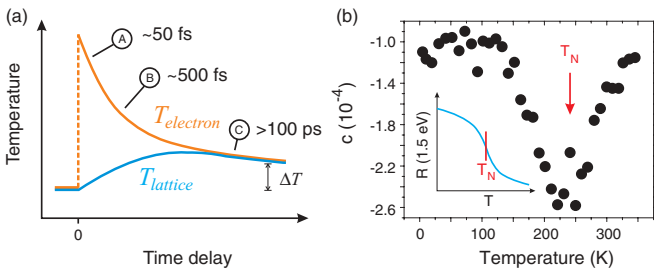

FIG. 5. (Color) (a) Diagram illustrating the temporal equilibration between the electronic and lattice subsystems following a pump pulse. The slowest process (C) is the cooling of the equilibrated system via diffusion of hot carriers or hot phonons away from the measured sample spot. (b) Temperature dependence of the offset (C) measured using a pump fluence of 15.4 μJ/cm^2. A clear minimum in C is observed at T_N corresponding to a rapid rise in reflectivity at 1.5 eV at T_N (see inset schematic). The errors in the fit parameters are less than the size of the symbols.

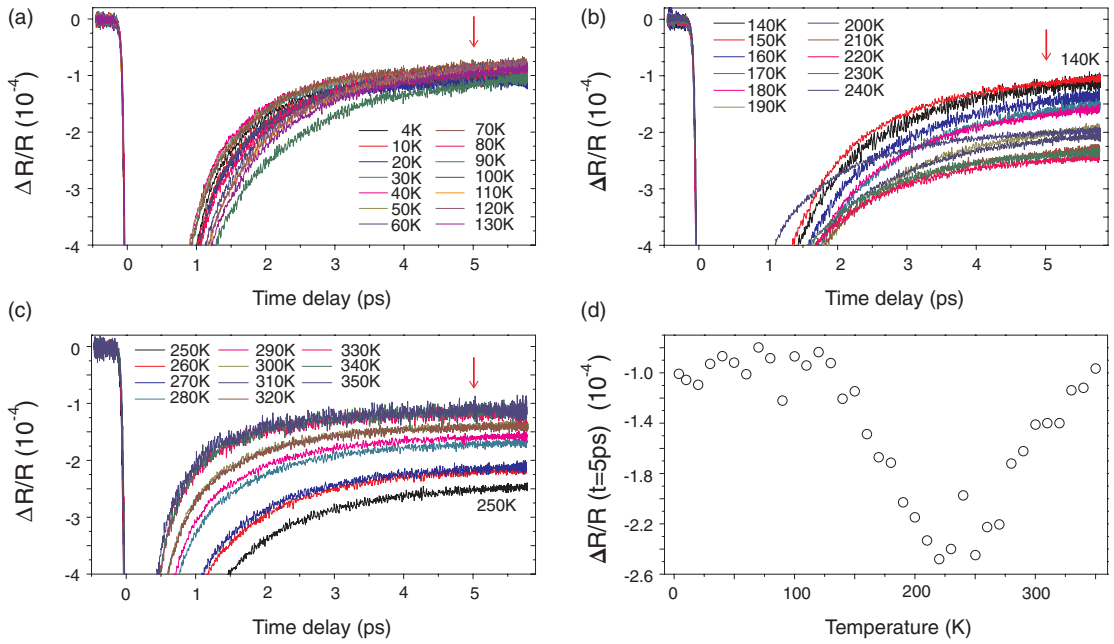

FIG. 6. (Color) Temperature dependence of un-normalized $\Delta R/R$ traces that are plotted over a range to emphasize the long time offset. Data are plotted from (a) $T = 4$–130 K, (b) 140–240 K, and (c) 250–350 K in increments of 10 K. (d) The value of $\Delta R/R$ at a time delay of 5 ps [red arrows in panels (a)–(c)] plotted as a function of temperature.

of hot carriers or hot phonons away from the laser illuminated area, which is estimated to well exceed 100 ps based on thermal conductivity and heat capacity data for Sr_2IrO_4.[16] To estimate the time required for heat to escape the laser excited region of the Sr_2IrO_4 crystal, we calculate its thermal diffusivity $D_{\rm th} = \frac{k}{\rho c}$ where k is the thermal conductivity, ρ is the density, and c is the specific heat. We use the values measured at $T = 100$ K in Ref. 16 of $k = 2.5$ W/m K, $\rho = 7440$ kg/m^3, and $c = 30$ J/kg K, which yields $D_{\rm th} = 1.1 \times 10^{-5}$ m^2/s. From this we estimate the time needed for heat to diffuse out of a 1-μm^2 area to be around 1 ns. Therefore to a very good approximation the offset C is a measure of the fractional change in reflectivity at 1.5 eV due to a small temperature change ΔT [Fig. 5(a)], namely $C = \frac{R(T+\Delta T)-R(T)}{R(T)}$. We estimate that at high pump fluences ΔT is of order 1 K because C is of order 10^{-4} and the fractional decrease in optical conductivity at 1.5 eV is estimated to be 2% from 10 to 500 K.[19] The ability to resolve such small temperature-induced changes in reflectivity is an advantage our nonequilibrium technique has over conventional equilibrium optical spectroscopy. Figure 5(b) shows that the temperature dependence of C exhibits a broad negative peak with an extremum exactly at T_N, which indicates that a small temperature rise causes the largest decrease of the 1.5-eV reflectivity exactly at T_N. From this we can infer a broad temperature window ($0.6 \lesssim T/T_N \lesssim 1.4$) within which R (1.5 eV) starts to rise sharply with cooling, with the greatest slope occurring at T_N [inset Fig. 5(b)]. The fact that this temperature window largely coincides with that over which τ_2 increases most drastically [Fig. 4(d)] is consistent with a Mott-Hubbard mechanism where spectral weight is transferred from low in-gap energies ($\sim$0.1 eV[12]) to energies (1.5 eV) far exceeding it.

To demonstrate that this behavior is independent of our fitting procedure, we show that the temperature dependence of the long time offset in $\Delta R/R$, the asymptotic value of the un-normalized reflectivity variation after the first two fast decay processes, can be obtained even without fitting. Figure 6(a) shows that between $T = 4$ and 130 K, this asymptotic value does not show a measurable systematic variation with temperature. Upon heating from 140 to 240 K [Fig. 6(b)], the offset clearly decreases with heating and upon heating further from 250 to 350 K [Fig. 6(c)], the offset exhibits a clear increase with heating. By plotting the value of $\Delta R/R$ at 5 ps as a function of temperature [Fig. 6(d)], we can already visualize the temperature dependence of the offset, which is very similar to that obtained through fitting [Fig. 5(b)]. This proves that the peak observed at T_N in the offset C is independent of how we fit the initial fast dynamics.

We note that variations in reflectivity can also be caused by a narrowing or shift of Lorentz oscillators representing direct optical transitions at 1.5 eV that do not involve spectral weight redistribution, and that our measurements do not distinguish between density of states changes in the occupied $J_{\rm eff} = 3/2$ and $J_{\rm eff} = 1/2$ initial states versus the unoccupied $J_{\rm eff} = 1/2$ final state. However, there is no current explanation for how such changes can be induced via magnetic ordering in the $J_{\rm eff} = 1/2$ band. Regardless, the observed temperature dependence of the quasiequilibrium reflectivity at 1.5 eV is unusual because the relaxation rate behavior suggests a Slater-type behavior (Fig. 4), which should be dominated by low-energy physics near the Fermi level and have little effect on the high-energy reflectivity.

IV. CONCLUSIONS

Our results taken altogether suggest that unlike La_2CuO_4, which remains a Mott insulator far above its magnetic ordering

temperature, Sr_2IrO_4 undergoes a metal-to-insulator transition across T_N. This suggests that Sr_2IrO_4 is more accurately described as an intermediate coupling ($U \approx W$) insulator that exhibits both Mott-Hubbard and Slater-type characteristics. Our observation that this metal-to-insulator transition takes place over a wide temperature window compared to T_N naturally explains the lack of sharp anomalies at T_N in transport, thermodynamic, and optical conductivity data. We argue that these may be signatures of a rare example of a temperature-controlled continuous metal-to-insulator transition in a quasi-two-dimensional system hitherto unobserved in any d-electron material,[28] and may also be applicable to the wider class of $J_{\text{eff}} = 1/2$ Mott insulating perovskite, honeycomb, hyperkagome, and pyrochlore iridates. Moreover, transport data on $5d$ Os oxides suggestive of continuous metal-to-insulators transitions[32] show that the confluence of strong spin-orbit coupling and on-site Coulomb interactions is a general playground for unconventional metal-to-insulator transitions.

ACKNOWLEDGMENTS

We thank F. Wang, T. Senthil, A. Vishwanath, S. Kehrein, K. Michaeli, R. Flint, S. Drapcho, and Y. Wang for useful discussions. N.G. acknowledges support from Army Research Office Grant No. W911NF-11-1-0331. C.G. acknowledges support through National Science Foundation Grants No. DMR-0856234 and No. EPS-0814194.

[1] B. J. Kim *et al*., Phys. Rev. Lett. **101**, 076402 (2008).
[2] H. Okabe, N. Takeshita, M. Isobe, E. Takayama-Muromachi, T. Muranaka, and J. Akimitsu, Phys. Rev. B **84**, 115127 (2011).
[3] G. Cao, J. Bolivar, S. McCall, J. E. Crow, and R. P. Guertin, Phys. Rev. B **57**, R11039 (1998).
[4] D. Pesin and L. Balents, Nat. Phys. **6**, 376 (2010).
[5] B.-J. Yang and Y. B. Kim, Phys. Rev. B **82**, 085111 (2010).
[6] X. Wan, A. M. Turner, A. Vishwanath, and S. Y. Savrasov, Phys. Rev. B **83**, 205101 (2011).
[7] M. J. Lawler, H.-Y. Kee, Y. B. Kim, and A. Vishwanath, Phys. Rev. Lett. **100**, 227201 (2008).
[8] Y.-Z. You, I. Kimchi, and A. Vishwanath, arXiv:1109.4155.
[9] F. Wang and T. Senthil, Phys. Rev. Lett. **106**, 136402 (2011).
[10] C. Martins, M. Aichhorn, L. Vaugier, and S. Biermann, Phys. Rev. Lett. **107**, 266404 (2011).
[11] B. J. Kim, H. Ohsumi, T. Komesu, S. Sakai, T. Morita, H. Takagi, and T. Arima, Science **323**, 1329 (2009).
[12] H. Watanabe, T. Shirakawa, and S. Yunoki, Phys. Rev. Lett. **105**, 216410 (2010); H. Jin, H. Jeong, T. Ozaki, and J. Yu, Phys. Rev. B **80**, 075112 (2009).
[13] R. Arita, J. Kunes, A. V. Kozhevnikov, A. G. Eguiluz, and M. Imada, Phys. Rev. Lett. **108**, 086403 (2012).
[14] G. Jackeli and G. Khaliullin, Phys. Rev. Lett. **102**, 017205 (2009).
[15] N. F. Mott, *Metal-Insulator Transitions* (Taylor & Francis, London, 1990); F. Gebhard, *The Mott Metal-Insulator Transition* (Springer, Berlin, 1997).
[16] N. S. Kini, A. M. Strydom, H. S. Jeevan, C. Geibel, and S. Ramakrishnan, J. Phys.: Condens. Matter **18**, 8205 (2006).
[17] S. Chikara, O. Korneta, W. P. Crummett, L. E. DeLong, P. Schlottmann, and G. Cao, Phys. Rev. B **80**, 140407(R) (2009).
[18] M. Ge, T. F. Qi, O. B. Korneta, D. E. DeLong, P. Schlottmann, W. P. Crummett, and G. Cao, Phys. Rev. B **84**, 100402(R) (2011).
[19] S. J. Moon, H. Jin, W. S. Choi, J. S. Lee, S. S. A. Seo, J. Yu, G. Cao, T. W. Noh, and Y. S. Lee, Phys. Rev. B **80**, 195110 (2009).
[20] N. Gedik, P. Blake, R. C. Spitzer, J. Orenstein, R. Liang, D. A. Bonn, and W. N. Hardy, Phys. Rev. B **70**, 014504 (2004).
[21] E. E. M. Chia, J. X. Zhu, H. J. Lee, N. Hur, N. O. Moreno, E. D. Bauer, T. Durakiewicz, R. D. Averitt, J. L. Sarrao, and A. J. Taylor, Phys. Rev. B **74**, 140409(R) (2006).
[22] J. Hohlfeld, J. G. Müller, S.-S. Wellershoff, and E. Matthias, Appl. Phys. B **64**, 387 (1997).
[23] I. Simon, J. Opt. Soc. Am. **41**, 336 (1951).
[24] H. J. Bowlden and J. K. Wilmshurst, J. Opt. Soc. Am. **53**, 1073 (1963).
[25] J. S. Lee, Y. Krockenberger, K. S. Takahashi, M. Kawasaki, and Y. Tokura, Phys. Rev. B **85**, 035101 (2012).
[26] A. Rothwarf and B. N. Taylor, Phys. Rev. Lett. **19**, 27 (1967).
[27] H. Okamoto, T. Miyagoe, K. Kobayashi, H. Uemura, H. Nishioka, H. Matsuzaki, A. Sawa, and Y. Tokura, Phys. Rev. B **83**, 125102 (2011).
[28] M. Imada, A. Fujimori, and Y. Tokura, Rev. Mod. Phys. **70**, 1039 (1998).
[29] S. Lupi *et al*., Nature Comm. **1**, 105 (2010).
[30] S. Fujiyama, H. Ohsumi, T. Komesu, J. Matsuno, B. J. Kim, M. Takata, T. Arima, and H. Takagi, Phys. Rev. Lett. **108**, 247212 (2012).
[31] G. Kotliar and D. Vollhardt, Phys. Today **57**(3), 53 (2004).
[32] D. Mandrus, J. R. Thompson, R. Gaal, L. Forro, J. C. Bryan, B. C. Chakoumakos, L. M. Woods, B. C. Sales, R. S. Fishman, and V. Keppens, Phys. Rev. B **63**, 195104 (2001); Y. G. Shi *et al*., *ibid*. **80**, 161104(R) (2009).

Confinement-Deconfinement Transition as an Indication of Spin-Liquid-Type Behavior in Na_2IrO_3

Zhanybek Alpichshev,[1] Fahad Mahmood,[1] Gang Cao,[2] and Nuh Gedik[1,*]
[1]Department of Physics, Massachusetts Institute of Technology, Cambridge, Massachusetts 02139, USA
[2]Department of Physics and Astronomy, University of Kentucky, Lexington, Kentucky 40506, USA
(Received 7 May 2014; published 7 January 2015)

We use ultrafast optical spectroscopy to observe binding of charged single-particle excitations (SE) in the magnetically frustrated Mott insulator Na_2IrO_3. Above the antiferromagnetic ordering temperature (T_N) the system response is due to both Hubbard excitons (HE) and their constituent unpaired SE. The SE response becomes strongly suppressed immediately below T_N. We argue that this increase in binding energy is due to a unique interplay between the frustrated Kitaev and the weak Heisenberg-type ordering term in the Hamiltonian, mediating an effective interaction between the spin-singlet SE. This interaction grows with distance causing the SE to become trapped in the HE, similar to quark confinement inside hadrons. This binding of charged particles, induced by magnetic ordering, is a result of a confinement-deconfinement transition of spin excitations. This observation provides evidence for spin liquid type behavior which is expected in Na_2IrO_3.

DOI: 10.1103/PhysRevLett.114.017203 PACS numbers: 75.10.Kt, 71.10.Li, 78.47.jj

Spin-orbit coupling (SOC) can give rise to highly nontrivial physics. Prime examples of the role of SOC in condensed matter systems are the topological insulators which have a nontrivial topology of their band structure due to sufficiently strong SOC [1,2]. In the case of simpler "band topological insulators," the gap is determined by the spin-orbit coupling and the system can be treated as noninteracting. These materials have been subject to intensive research and are relatively well understood. Much less clear is the situation in which the insulating state before the "turning on" of SOC was not a trivial band insulator but an insulator with a gap driven by electron-electron interactions, such as a Mott insulator.

Iridate compounds belong to the class of materials in which electron-electron interactions play an essential role. Expected to be metallic based on a simple electron count, these systems are insulators exhibiting Mott-type behavior. On the other hand, due to the extended nature of the $5d$ orbitals, the on-site Coulomb repulsion has a moderate value ($U \approx 0.4$–2.5 eV) and SOC ($\approx$0.4–1 eV) effectively competes with electron-electron interactions [3].

One of the most intriguing proposals of novel physics made for iridate compounds was that the interplay between spin-orbit interactions, crystal field splitting, and Coulomb repulsion of $5d$ electrons in Na_2IrO_3 can lead to a formation of effective moments with $J_{\text{eff}} = 1/2$ on every Ir-O octahedron with highly anisotropic nearest neighbor coupling. This coupling has a very special form and, given its layered quasi-2D honeycomb lattice structure, was proposed [4–7] to be a solid-state realization of the Kitaev model [8] of a spin liquid.

The real Hamiltonian of Na_2IrO_3 is, however, not a pure Kitaev model and should also have conventional terms such as Heisenberg-type exchange interaction between effective moments. Such terms generally spoil the symmetry of the pure Kitaev model and result in an ordered ground state [5,7,9] in the limit of low temperatures. The structure of the ground state should then depend on the details of the extra term in the Hamiltonian. Neutron studies [10–12] have revealed that Na_2IrO_3 has an antiferromagnetic ground state of "zigzag" type [Fig. 3(b)] with a Néel temperature of $T_N = 15.3$ K. The minimal Hamiltonian within the framework of the modified Kitaev model that can give such a ground state consists of an antiferromagnetic Kitaev term and a ferromagnetic Heisenberg term [5,7,9,13]. Although Na_2IrO_3 is not a quantum spin liquid, the fact that the ordering temperature $T_N = 15$ K is considerably smaller than both the Curie-Weiss temperature $T_\Theta = -125$ K [7] and the spin wave energy $E_{\text{sw}} \sim 5$ meV [10] implies that the degree of frustration is still quite strong and the Kitaev term should dominate the low-energy physics. Nevertheless, despite intensive research performed on Na_2IrO_3 thus far, to the best of our knowledge, there has been no evidence of the spin-liquid-type behavior in this material, which should show up in the $T_N \ll T \ll T_\Theta$ temperature range [14].

In this Letter we report our results on ultrafast studies of photoexcitations in Na_2IrO_3. We observe a change in their dynamics across Néel temperature; namely, we observe a sharp increase in the binding energy of the excitons that they form as the system enters the ordered phase. We interpret this as evidence of confinement-deconfinement transition of spin and charge excitations across T_N, which is a hallmark of spin-liquid physics [15,16].

Time-resolved experiments were performed with a Ti: sapphire oscillator lasing at the center wavelength of

795 nm ($\hbar\omega = 1.55$ eV) producing pulses of 60 fs in duration. The repetition rate of the laser was reduced to 1.6 MHz with an external pulse picker to avoid cumulative heating effects on the sample, and the spot size of a spatially Gaussian beam was set to 60 μm FWHM. Single crystals of Na_2IrO_3 were grown using a self-flux method from off-stoichiometric quantities of IrO_2 and Na_2CO_3. Similar technical details were described elsewhere [17–19].

Data were obtained with a standard optical pump-probe technique [20,21] where a single "pump" pulse excites the sample and the resulting dynamical response is monitored by the normalized change in the reflectivity $\Delta R(t)/R$ of a separate "probe" beam as a function of time delay Δt between the pump and probe. We use the same wavelength for both pump and probe pulses. For phase-sensitive measurements a variation of the pump-probe technique called the "heterodyne transient grating" (HTG) method is used [22]. This method, unlike the pump-probe technique, can distinguish between components of ΔR with different physical origins [23]. Here an interference of two pump beams produces a spatially modulated excitation pattern which is studied by a probe beam diffracted off the sample. The diffracted beam is then heterodyned with an additional beam used as a local oscillator. The time dependence $\Delta R(t)$ of a multicomponent system response obtained in this way changes as a function of the phase difference ϕ between the probe beam and the local oscillator, whereas that of a single-component system just scales proportionally to $\cos(\phi)$ (also see the Supplemental Material [24]).

Given the band structure of Na_2IrO_3 [26–28] [Fig. 1(a)], the absorption of a pump photon with energy E eV causes electrons to transition from a $J_{\text{eff}} = 3/2$ band into the upper Hubbard band, which is the only accessible level for the excited electrons for this photon energy. The depleted valence band is then partially refilled through relaxation of the photoexcited electrons and partially with electrons from the lower Hubbard band [Fig. 1(a)]. At the end of this relatively fast process the system will have some amount of excitations in the upper Hubbard band (double occupancies in real space or "doublons") and an equal amount of holes in the lower Hubbard band. The excited state is metastable as the optical dipole transitions within the Hubbard band are prohibited by selection rules ($\Delta J = 0$ transition). Moreover, the energy of the magnons, which are the relevant excitations $\epsilon \approx 5$–10 meV $\sim k_B T_\Theta$ [10], is much less than the Hubbard gap $U \sim 350$ meV, which is the energy which needs to be dissipated during the doublon-hole recombination process, making the lifetime exponentially large in U/ϵ [29]. This observation allows us to consider holes and doublons as stable quasiparticles for the time scales relevant to our experiments (~100 ps).

Figures 1(b) and 1(c) show HTG data taken at a pump fluence of ~9.5 μJ/cm^2 for various values of ϕ at 295 and 25 K, respectively. At each temperature the shape of the differential reflectivity time trace $\Delta R(t)/R$ with time changes as ϕ is varied, indicating that there is more than one component in the system response. This behavior is in agreement with earlier resonant inelastic x-ray scattering (RIXS) studies [26,30], which demonstrated that the low-energy excitations of Na_2IrO_3 are single-particle (doublons and holes) excitations (SE) and their bound state is known as a Hubbard exciton (HE) [31]. Figures 3(a) and 3(b) demonstrate that the component featuring the fast spike near $t = 0$ is clearly getting stronger with increasing temperature, allowing us to identify it with SE. This is similar to the results of studies of photoexcited Mott insulators in other systems [31] where the $\Delta R/R$ component with an initial fast spike was shown to be due to SE whereas the one without is due to HE.

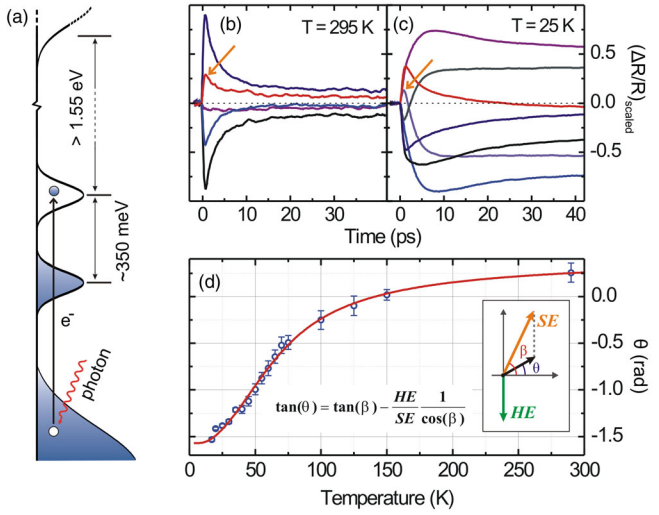

FIG. 1 (color online). (a) Sketch of the band structure of Na_2IrO_3 illustrating the relevant processes during photoexcitation with 1.5 eV light. (b) HTG traces for selected values of ϕ (see text) at a pump fluence of 9.5 μJ/cm^2 at $T = 295$ K and (c) at $T = 25$ K. Note the multicomponent behavior of the HTG traces as a function of ϕ and the relative strengthening of the initial spike (labeled with an arrow) associated with single-particle excitations (SE) at higher temperature (see text). (d) Phase (θ) of the total signal at $t \approx 50$ ps in the quasiequilibrium state as a function of temperature. Error bars represent the 95% confidence interval (2 s.d.) in extracting the phase. Solid red line is a fit to the data based on the Boltzmann distribution of SE and Hubbard exciton (HE) populations, $\text{SE/HE} \propto \exp(-\Delta/k_B T)$. Inset: Phasor diagram representing quasiequilibrium ΔR (black phasor) due to SE and HE.

It should be noted that both components (SE and HE) are long-lived and thus they both contribute to the composition of the total signal in the long-time limit. There, a quasi-thermal equilibrium is established between SE and HE and thus their population ratio should be proportional to the Boltzmann factor $\exp(-\Delta/k_B T)$, where Δ is the HE binding energy. In this regime, the net phase θ of the signal response reaches a constant value that is directly related to the quasiequilibrium population ratio of SE and HE (see

the inset of Fig. 1(d) and the Supplemental Material [24]). This phase θ is plotted in Fig. 1(d) as a function of temperature from which we extract $\Delta \approx 4.6 \pm 0.8$ meV. This value is within the bounds set by RIXS measurements [26] and confirms that the component featuring a fast spike at $t = 0$ is indeed due to SE. Figures 2(a) and 2(b) show the HTG data taken for a very low pump fluence of value of ~ 30 nJ/cm^2 at temperatures above and below T_N, respectively. Similar to the higher fluence data, the low fluence response above T_N [Fig. 2(a)] clearly features more than one component, indicating the presence of both SE and HE. On the other hand, the low fluence response below T_N [Fig. 2(b)], strikingly, scales proportionally to $\cos(\phi)$, implying a single-component behavior, which, as discussed above, is due to Hubbard excitons.

We now proceed to study this disappearance of SE as a function of temperature by performing optical pump-probe measurements for low excitation densities to minimize heating effects. Figure 2(d) shows reflectivity transients for various temperatures below T_N for two different pump fluences. As can be seen, the normalized system response

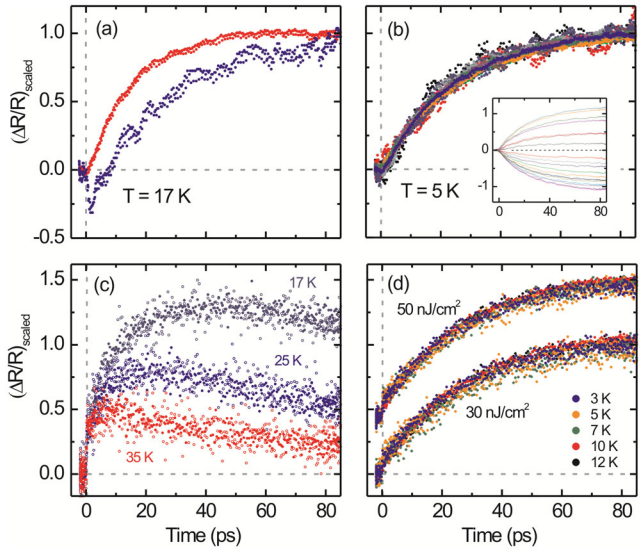

FIG. 2 (color online). HTG and pump-probe data at various temperatures at low pump fluence. (a) Representative HTG traces at $T = 17$ K for two different values of ϕ at a pump fluence of 30 nJ/cm^2. The traces exhibit qualitatively different shapes indicating the presence of both SE and HE. Note the fast spike around $t = 0$ for the purple curve. This is signature of SE (see Fig. 1 and text). (b) HTG traces at $T = 5$ K for 19 different values of ϕ at a pump fluence of 30 nJ/cm^2, scaled to emphasize the single component (HE) nature of the response. Inset: Unscaled HTG traces. (c) Scaled $\Delta R/R$ traces for temperatures above T_N ($T = 17$, 25, and 35 K) at different fluences: 100 nJ/cm^2 (filled markers) and 50 nJ/cm^2 (open markers). Note the strong temperature dependence and the lack of fluence dependence in this limit. (d) $\Delta R/R$ traces for temperatures below T_N ($T = 5$, 7, 10, and 12 K), scaled to emphasize the universal behavior of transient traces. Upper curve, 50 nJ/cm^2; lower curve, 30 nJ/cm^2. Curves at different fluence values are shifted for better clarity.

in this regime is independent of both temperature and pump fluence, demonstrating that the single-component behavior observed at $T = 5$ K persists up to T_N. This indicates that SEs are suppressed throughout the ordered phase. On the contrary, reflectivity transients above T_N [Fig. 2(c)] strongly depend on temperature, which combined with the HTG data (Fig. 1) indicate the formation and strengthening of the component due to SE. Moreover, above T_N, the normalized transients at each temperature are independent of pump fluence [Fig. 2(c)], demonstrating that the relative composition of the signal (ratio between SE and HE populations) is constant as a function of pump fluence in this low excitation density regime. This sudden disappearance of SE at T_N implies a sharp increase in the HE binding energy.

In general, an increase in binding energy of an exciton can be either due to an enhancement of the attracting potential or due to "slowing down" of the overall dynamics, e.g., by increasing the effective mass. The effective mass of a single hole in a Mott insulator is indeed enhanced due to emission of magnons, but this happens in both the antiferromagnetic and disordered phases [32]. But more importantly, it is the sheer disparity between the bandwidth of the single-particle excitations ($\gtrsim 100$ meV, e.g., Ref. [26]) and the Heisenberg coupling responsible for antiferromagnetism ($\sim k_B T_N \approx 1$ meV) that makes the slowing-down scenario unlikely. Therefore, we conclude that the increase in binding energy of HE is a result of enhancement in attraction between SEs.

Here we present a simple intuitive picture of the effective attraction mediated by antiferromagnetic ordering responsible for additional binding energy, based on the Kitaev-Heisenberg model. This Hamiltonian naturally gives rise to the zigzag order [9]:

$$H_{\mathrm{KH}} = J_K \sum_{\langle ij \rangle} S_i^l S_j^l + J_H \sum_{\langle ij \rangle} \vec{S}_i \cdot \vec{S}_j. \qquad (1)$$

The main term here is the strongly frustrated Kitaev term ($T_\Theta = -125$ K). The Heisenberg term lifts the degeneracy and the system "freezes" into an ordered state below T_N. In the zigzag phase every spin finds its "Kitaev partner" and antialigns itself with the spin of its partner in the direction determined by the orientation of the connecting bond. The much smaller Heisenberg term ($T_N = 15.3$ K) tries to minimize its energy under the condition that every spin has a Kitaev partner. As can be seen in Fig. 3(b), the zigzag order satisfies this condition for all bonds except those that connect Kitaev partners.

This situation changes drastically when spinless defects such as doublons or holes are introduced into the system. These particles can be thought of as topological in the same sense as the excitations in the Rokhsar-Kivelson dimer model [33]. The spins that have lost their Kitaev partners reorganize the surrounding spin order at the expense of Heisenberg energy [Fig. 3(c)]. Reoriented spins form a

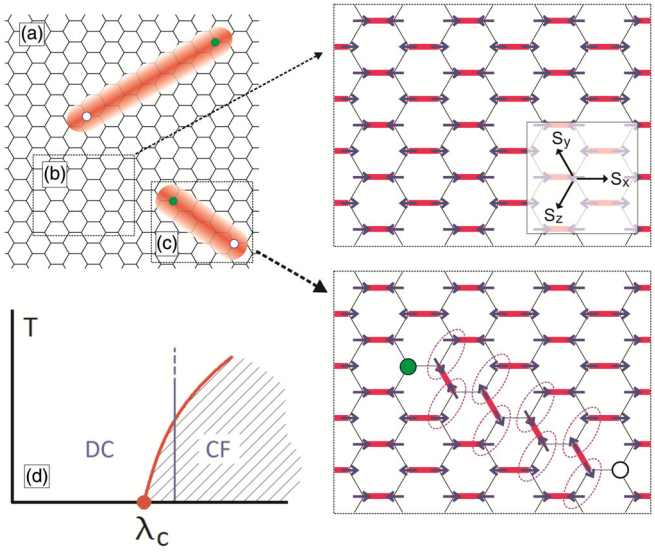

FIG. 3 (color online). (a) Schematic view of an excited sample. Green dots correspond to doublons while the white dots represent holes. The shaded red area marks the region where the spins are affected by the reconstruction, i.e., the "string" [see (c)]. (b) Sketch representing the zigzag ordered low temperature ground state. Red bonds connect Kitaev partners while gray bonds have a spin configuration that minimizes the Heisenberg energy. (c) Simplified representation of the restructured state with singlet defects (hole or doublon). The Heisenberg energy along the bonds highlighted by purple ovals is no longer minimal. The string composed of such bonds must begin and end on a defect. (d) Illustration of a phase diagram of a modified Kitaev model with a first-order quantum critical point and a phase boundary between confined (CF) and deconfined (DC).

string terminating on the other defect. The energy cost of this configuration is proportional to the number of broken Heisenberg links, which in turn is proportional to the length of the string connecting the two defects. This prohibits the long-range separation of the defects which, in the case of low excitation density, will predominantly be of opposite charges (doublon-hole), leading to an enhanced binding between them in addition to Coulomb attraction. This is similar to the picture of the quark confinement in high-energy physics [34]: separation of defects produces a string of perturbed vacuum between them with an energy proportional to its length. However, since breaking of this string in our case produces a pair of electrically neutral unpaired "dangling" spins (which *are* confined), the binding energy between doublons and holes is limited by the cost of breaking a Kitaev pair, which is of the order of Kitaev coupling, $J_K \approx 10$ meV in the case of Na_2IrO_3.

This is consistent with previous theoretical works on the Kitaev-Heisenberg model where it was observed that for sufficiently weak perturbations the Kitaev spin-liquid state persists, but as the extra term gets stronger, the system enters an ordered state [4,5,35]. Formulated in terms of spinons, such a transtition corresponds to the transition from a deconfined state (spin-liquid) to a confined state (antiferromagnet) [35,36]. This is a first-order phase transition [35,36], and no quantum critical region is expected above the quantum critical point $\lambda = \lambda_c$ [37], where λ is the relative strength of the Heisenberg term in the Hamiltonian. Therefore, confined and deconfined phases are separated by a simple boundary and the confinement-deconfinement transition can be observed not only by tuning the strength of the perturbing term λ at $T = 0$ as in Refs. [35,36], but also by going across the ordering temperature for a fixed $\lambda > \lambda_c$ [see Fig. 3(d)]. In the confined phase, all fractional excitations such as holons, doublons, and spinons are bound to each other and, conversely, can move independently in the deconfined phase [16].

The fact that the zigzag order is not a trivial antiferromagnet was evidenced in a recent work of Manni *et al.* [38], where partial substitution of Ir atoms with nonmagnetic Ti atoms resulted in the formation of a spin glass state at low temperatures. This has a natural explanation within our framework, as Ti sites can be treated as static spinless defects. At sufficient concentration they will be connected by spin strings as in Fig. 2(c). Since there are many different ways to connect different Ti sites, it is natural to expect a spin glass state at low temperatures.

In conclusion, we performed an optical pump-probe study of Na_2IrO_3, a material proposed to be a realization of the Kitaev model. We observed that photoinduced charged excitations display drastically different behavior below and above the Néel ordering temperature. Namely, the binding energy of the excitons that these particles form undergoes a sharp increase upon entering the ordered phase. Based on earlier theoretical studies on doped Mott insulators, we conjecture that this is due to an effective attraction brought about by the antiferromagnetic order rather than because of an increase in effective mass of quasiparticles. We argue that this attraction is a manifestation of confinement of spin excitations anticipated in the ordered phase of the Kitaev-Heisenberg model. Therefore, the change of behavior that we observe at the Néel temperature is due to the confinement-deconfinement transition, providing evidence of spin-liquid-type physics in Na_2IrO_3.

We thank Senthil Todadri, Patrick Lee, Subir Sachdev, and Maksym Serbyn for insightful discussions. This work was supported by the Army Research Office Grant No. W911NF-11-1-0331 (data taking and analysis), NSF Career Award No. DMR-0845296 (experimental setup), and the Alfred P. Sloan Foundation (theory and modeling). G. C. was supported by NSF Grants No. DMR-0856234 and No. DMR-1265162 (material growth).

*gedik@mit.edu

[1] M. Z. Hasan and C. Kane, Rev. Mod. Phys. **82**, 3045 (2010).
[2] X.-L. Qi and S.-C. Zhang, Rev. Mod. Phys. **83**, 1057 (2011).

[3] F. Ye, S. Chi, H. Cao, B. C. Chakoumakos, J. A. Fernandez-Baca, R. Custelcean, T. F. Qi, O. B. Korneta, and G. Cao, Phys. Rev. B **85**, 180403(R) (2012).
[4] G. Jackeli and G. Khaliullin, Phys. Rev. Lett. **102**, 017205 (2009).
[5] J. Chaloupka, G. Jackeli, and G. Khaliullin, Phys. Rev. Lett. **105**, 027204 (2010).
[6] Y. Singh and P. Gegenwart, Phys. Rev. B **82**, 064412 (2010).
[7] Y. Singh, S. Manni, J. Reuther, T. Berlijn, R. Thomale, W. Ku, S. Trebst, and P. Gegenwart, Phys. Rev. Lett. **108**, 127203 (2012).
[8] A. Kitaev, Ann. Phys. (Amsterdam) **321**, 2 (2006).
[9] J. Chaloupka, G. Jackeli, and G. Khaliullin, Phys. Rev. Lett. **110**, 097204 (2013).
[10] S. K. Choi *et al.*, Phys. Rev. Lett. **108**, 127204 (2012).
[11] X. Liu, T. Berlijn, W.-G. Yin, W. Ku, A. Tsvelik, Y.-J. Kim, H. Gretarsson, Y. Singh, P. Gegenwart, and J. P. Hill, Phys. Rev. B **83**, 220403 (2011).
[12] F. Ye, S. Chi, H. Cao, B. C. Chakoumakos, J. A. Fernandez-Baca, R. Custelcean, T. F. Qi, O. B. Korneta, and G. Cao, Phys. Rev. B **85**, 180403 (2012).
[13] J. G. Rau, E. Kin-Ho Lee, and H. Y. Kee, Phys. Rev. Lett. **112**, 077204 (2014).
[14] L. Balents, Nature (London) **464**, 199 (2010).
[15] S. Sachdev, Rev. Mod. Phys. **75**, 913 (2003).
[16] T. Senthil and M. P. A. Fisher, J. Phys. A **34**, L119 (2001).
[17] M. Ge, T. F. Qi, O. B. Korneta, D. E. De Long, P. Schlottmann, W. P. Crummett, and G. Cao, Phys. Rev. B **84**, 100402(R) (2011).
[18] S. Chikara, O. Korneta, W. Crummett, L. DeLong, P. Schlottmann, and G. Cao, Phys. Rev. B **80**, 140407(R) (2009).
[19] M. A. Laguna-Marco, D. Haskel, N. Souza-Neto, J. C. Lang, V. V. Krishnamurthy, S. Chikara, G. Cao, and M. van Veenendaal, Phys. Rev. Lett. **105**, 216407 (2010).
[20] J. Demsar, K. Biljakovic, and D. Mihailovic, Phys. Rev. Lett. **83**, 800 (1999).
[21] G. Segre, N. Gedik, J. Orenstein, D. Bonn, R. Liang, and W. Hardy, Phys. Rev. Lett. **88**, 137001 (2002).
[22] N. Gedik and J. Orenstein, Opt. Lett. **29**, 2109 (2004).
[23] J. P. Hinton, J. D. Koralek, Y. M. Lu, A. Vishwanath, J. Orenstein, D. A. Bonn, W. N. Hardy, and R. Liang, Phys. Rev. B **88**, 060508(R) (2013).
[24] See Supplemental Material at http://link.aps.org/supplemental/10.1103/PhysRevLett.114.017203, which includes [25], for more details on the experimental technique and sample preparation; and also includes additional arguments supporting main conclusions of the paper along with further discussion relevant to the physical picture presented in this Letter.
[25] G. M. Sheldrick, Acta Crystallogr. Sect. A **64**, 112 (2008).
[26] H. Gretarsson *et al.*, Phys. Rev. Lett. **110**, 076402 (2013).
[27] R. Comin *et al.*, Phys. Rev. Lett. **109**, 266406 (2012).
[28] C. H. Sohn *et al.*, Phys. Rev. B **88**, 085125 (2013).
[29] R. Sensarma, D. Pekker, E. Altman, E. Demler, N. Strohmaier, D. Greif, R. Jördens, L. Tarruell, H. Moritz, and T. Esslinger, Phys. Rev. B **82**, 224302 (2010).
[30] H. Gretarsson *et al.*, Phys. Rev. B **87**, 220407 (2013).
[31] F. Novelli, D. Fausti, J. Reul, F. Cilento, P. H. M. van Loosdrecht, A. A. Nugroho, T. T. M. Palstra, M. Gruninger, and F. Parmigiani, Phys. Rev. B **86**, 165135 (2012).
[32] C. L. Kane, P. A. Lee, and N. Read, Phys. Rev. B **39**, 6880 (1989).
[33] S. A. Kivelson, D. S. Rokhsar, and J. P. Sethna, Phys. Rev. B **35**, 8865 (1987).
[34] A. M. Polyakov, *Gauge Fields and Strings* (Harwood, Academic, Chur, Switzerland, 1987).
[35] R. Schaffer, S. Bhattacharjee, and Y. B. Kim, Phys. Rev. B **86**, 224417 (2012).
[36] S. Mandal, S. Bhattacharjee, K. Sengupta, R. Shankar, and G. Baskaran, Phys. Rev. B **84**, 155121 (2011).
[37] S. Sachdev, Nat. Phys. **4**, 173 (2008).
[38] S. Manni, Y. Tokiwa, and P. Gegenwart, Phys. Rev. B **89**, 241102(R) (2014).

Summary of our progress since PRL 114, 017203 (2015)

In our previous work which was published in PRL in January 2015, we have established that the interactions within Na-213 give rise to strongly frustrated Hamiltonian consistent with Kitaev-Heisenberg model, which among other things gives rise to spin-liquid type behavior in the disordered phase above Neel temperature. One of the open questions left in that work was the nature of the slow dynamics of the signal associated with the ordered phase. A detailed investigation of this question should have important implications for the very little understood problem of the non-equilibrium Mott insulating phase.

An implication of our work, which might give a hint on what is going on during the slow (tens-of-picoseconds-scale) evolution of the system, was that in the presence of defects (either permanent defects or transient ones, such as slow photo-excitations) the low-temperature phase of Na-213 should exhibit spin-glass behavior. The slow process that we observe might therefore be the relaxation of a spin-glass. The reason why the timescales we observe in our pump-probe experiments are short for a spin-glass, are then due to the fact that the disorder due to photo-induced carriers is not a perfectly quenched disorder.

In order to investigate the nature of the low temperature phase of a frustrated Mott insulator Na-213 we have built a special three pulse pump-probe setup, with two beams for pumping and one for probing. According to our design one of the pump beams has a wavelength of 800nm to make a connection with previous experiments. As before this pulse couples most efficiently to electronic degrees of freedom. On the other hand the other pump beam is deep inside the infrared spectrum (2100nm). This beam energy corresponds to forbidden frequency range for electronic transitions in Na-213, and therefore mostly couples to non-electronic degrees of freedom such as phonons and from the point of view of electrons, only produces perturbations in temperature. With this setup we could do an ultrafast analog of classical experiments of M. Lederman *et al.* and M. Ocio *et al.*, on spin glasses.

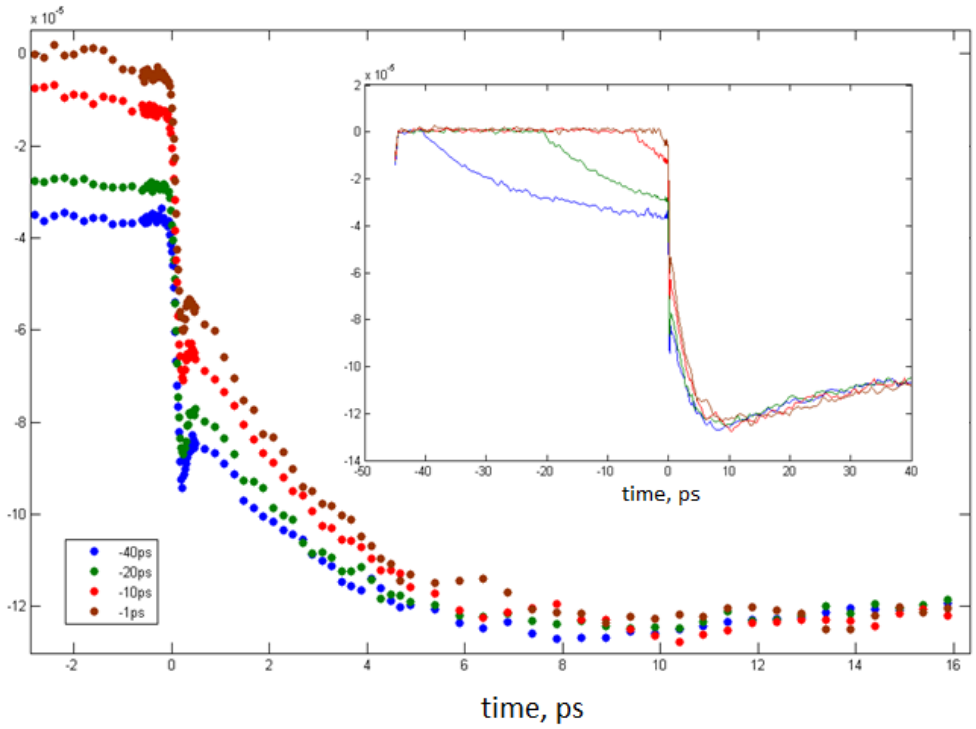

On the figure above we show our preliminary result. The horizontal axis on both plots (main panel and inset) corresponds to the time delay between the 2100nm pump pulse and the 900nm probe pulse (we chose this wavelength over usual 800nm to avoid excessive pump scattering). The inset panel shows the full measured time range and the main panel shows the zoom onto the region around the time of arrival of the 2100nm pulse. Different curves correspond to different times of arrival of the 800nm pump relative to the 2100nm one. The first thing to notice on the main panel is that after the second pump pulse (2100nm) the system "remembers" its previous history for a while. This is consistent with our expectations that 2100nm pulse only induces sudden temperature increase without affecting electronic distribution. But the most important message of the figure is that although the delay between 800nm and 2100nm pulse can be as large as 40ps (see inset), the history *does* get forgotten completely within less than 10ps.

If our picture correct, then what we observe in our regular pump-probe experiments is the relaxation of a spin glass. Moreover in our three-pulse measurements we observe the "forgetting" effect of a spin glass in real time. The comparison of the characteristic time of "forgetting" with the magnitudes of available physical parameters of Na-213 further support this picture. Indeed, quasi-classically, the low energy dynamics of the Kitaev-Heisenberg model can be thought of as fluctuating "hard" dimers formed by strong Kitaev term weakly interacting among each other through Heisenberg energy. Therefore it is the Heisenberg energy ($J_K \sim T_{Neel} \sim 1$ps) which is responsible for the dimer dynamics, and ultimately the relaxation times.